Korea-Australia Rheology Journal, Vol.26, No.2, pp.149-158 (May 2014) www.springer.com/13367
DOI: 10.1007/s13367-014-0015-3

Experimental and modeling study of viscoelastic behaviors of magneto-rheological shear thickening fluids

Gang Rou Peng[1], Weihua Li[1,*], Tong Fei Tian[1], Jie Ding[2,*] and Masami Nakano[3]

[1]*School of Mechanical, Materials and Mechatronic Engineering, University of Wollongong, Wollongong, NSW 2522, Australia*
[2]*Land Division, Defence Science and Technology Organisation, 506 Lorimer Street, Fishermans Bend, VIC 3207, Australia*
[3]*Intelligent Fluid Control Laboratory, Institute of Fluid Science, Tohoku University, 2-1-1 Katahira, Aoba-ku, Sendai 980-8577, Japan*

(Received November 18, 2013; final revision February 25, 2014; accepted March 3, 2014)

Nowadays, both Magneto-rheological Fluid (MRF) and Shear Thickening Fluid (STF) have separately attracted considerable interest due to the fast reversible response to either external magnetic field or abrupt shearing loading. In this paper, we fabricated a combined phase of Magneto-rheological Shear Thickening Fluid (MRSTF), where the 25 wt% STF is applied as medium phase with the addition of varied fractions of iron particle. The investigation of the dynamic behavior of this novel material under oscillatory shear was launched in a parallel-plate rheometer. The relevance of the dynamic behavior to strain amplitude, frequency and external magnetic field were investigated and discussed. A four-parameter viscoelastic model was applied to reconstruct the mechanical behavior of the MRSTF under different working conditions, and the parameters were identified within the Matlab optimization algorithm. The comparison between the experimental data and the model prediction results indicated that the four-parameter model could predict viscoelastic material with desired accuracy. The MRSTF exhibits features of both components, while prone more to MRF with the inception of external field excitations.

Keywords: shear thickening fluids, oscillatory, modeling

1. Introduction

Magneto-rheological Fluids (MRFs) refer to the kind of fluids whose mechanical behavior can be manipulated by an external magnetic field (Carlson *et.al,* 1995; Liu *et al*., 2005; Park *et al.,* 2010). When the material is subjected to the flux densities, the apparent viscosities for typical MRFs can increase as high as several orders of magnitude in matter of milli-seconds (de Vicente *et al*., 2011). Featuring controlled viscosities, the MRF is of attractive candidate for applications in mechanical systems that involve vibration attenuation and torque transmission, for instance, shock absorbers, brakes, clutches and artificial joints (Milecki *et al*., 2012; Zhu *et al*., 2012; R.Russo and M.Terzo, 2011; Kikuchi *et al*., 2011; Dong *et al*., 2006). Conventionally speaking, the MRFs consist of two-phases: the micro-sized magnetic ferro-particles, a carrier fluid, usually non-magnetical with mineral and silicone oils being the most commonly used and some additives in case of sediments (Rankin *et al*., 1999).

When all the approaches mentioned above have a common trait that an external power source is required for activation, a novel class of materials, the Shearing Thickening Fluids (STFs), exhibit potential for changing properties with respect to loading conditions with no external power sources. STFs are functioned by concentrated colloidal suspension in fluids, which increase sharply with viscosity when the applied shear rate is beyond a critical point. Having said that, the increased viscosity is observed as both passively activated as well as reversible (M.R. Jolly and J.W. Bender, 2006; Fischer *et al.,* 2006).

The two most accepted mechanisms behind the shear thickening phenomenon are: Order-Disorder Transition and Hydro-Cluster Formation. In the former mechanism, it was found that the fact that the onset of the shear thickening phenomenon both continuous and discontinuous coincides with a transition in the microstructure from ordered, hexagonally packed layers at comparatively lower shear to a disordered state at a higher shear rate, which signals obvious shear thickening phenomenon as the viscosity exhibits a dramatic increase (Bender *et al.,* 1995). While the latter mechanism stated that the particles inside of the liquid system are pushed into each other by shear, and to move away from each other they must overcome the viscous drag forces from the small lubrication gaps between neighboring particles. This suggests a critical shear rate above which particles stick together transiently by the lubrication forces and can grow into larger clusters. Then with the increase of shear rate, most particles are no longer independent of each other, thus resulting in growing aggregation which can jam the flow in the fluid (Egres *et al.,* 2006).

STFs have huge potential for in industrial applications;

*Corresponding authors: weihuali@uow.edu.au;
Jie.Ding@dsto.defence.gov.au

large numbers of patents are issued to both specific application and preparation of the STFs themselves. Just to mention a few, the devices with adaptive stiffness of damping (Zhang *et al.,* 2008), smart structures (Neagu *et al.,* 2009) and body armor (Kalman, 2010).

STFs and MRFs, have been extensively investigated and some researchers have already tried to present both functions in a joint manner (Zhang *et al.,* 2008; Yu *et al.,* 2010), yet the viscoelastic property was not discussed in details. In this paper, the advantages of both MRFs and STFs are jointly presented in details by adding iron powder into the base medium of STF, and the resultant sample possessed reasonable passive response as well as controllable MR effect in case of varied external magnetic fields.

Materials displayed dynamic viscoelastic properties, including parameters like storage modulus, loss modulus and loss factor, which are defined in a linear viscoelastic (LVE) range with clear physical meaning, in which the response stress of viscoelastic materials for sinusoidal strain loading is also sinusoidal. In contrast, when the strain amplitude is above the LVE range, namely non-linear viscoelastic (NLVE) range, high order harmonics would start to appear and the stress response is no longer in tune with the original strain excitation (McKinley *et al.,* 2008). Consequently, the transform from LVE to the NLVE range sees significant difference with the dynamic properties and the existing parameters are no longer physically meaningful due to the non-linear stress response (Ahn *et al.,* 2005; Wang *et al.,* 2009).

Large amplitude oscillatory shear (LAOS) is a commonly used method to determine the transition between LVE and NLVE ranges (Gong *et al.,* 2012; Li *et al*., 2003). When the strain amplitude is small and within the LVE range, the storage modulus is independent of the strain deformation, oppositely, as the amplitude increases beyond the LVE range, an obvious decrease in such parameters is observed (Sun *et al.,* 2011), within this variation, one can easily recognize the LVE range.

Another effective method of analyzing the transition between the LVE range and the NLVE range is by examining the shape of the strain-stress hysteresis loop (Lissajous Curve) (Kim *et al.,* 2002; Petekidis *et al*., 2010). When the actuating strain is within the LVE range, the strain-stress hysteresis loop exhibits an elliptical shape, while a non-elliptical curve would appear as the outcome of high order harmonics of the corresponding shear stress in the case of an NLVE range (Li *et al.,* 2010; Ng *et al.,* 2011).

In summary, LAOS testing should reveal a different aspect of material behavior, as the deformation is extended to nonlinear regime, thus it is of more interest in the study of NLVE in suspensions, as we will unfold in a later part of this paper.

2. Experimental

2.1. Fabrication of Both STF Medium and MRSTF

The STF was used as the base material, where it is composed of hydrophilic fumed silica (S5505, from Sigma-Aldrich used as received) of a primary size of 14 nm and carrier fluid of ethylene glycol [$HOCH_2$ CH_2OH] (102466, ReagentPlus, from Sigma-Aldrich). In the fabrication process, the carrier fluid was added to the fumed silica powder and mechanically stirred for approximately 2 h. After the stirring, the dispersed sample was placed in a vacuum oven for several hours to eliminate air bubbles. In this case a 25% wt fraction sample was selected for study.

Carbonyl iron particles (C3518, from Sigma-Aldrich) with 5 μm mean particle size were added to the prepared STF base to generate target MRSTF samples, the sample fraction generated was 5% (Zhang *et al.* 2008), as the higher iron particle fraction would result in dominant MR behavior. The iron particles were mixed with STF and have the mixture manually stirred for 10 min, then the air bubbles were removed in a vacuum oven before tests were launched.

Through this fabrication process, the MRSTF sample was generated in a very stable form, and no supernatant or phase separation was observed even after a few weeks.

2.2. Rheological Testing

A parallel-plate stress controlled rheometer MCR 301 was used with a constant gap of 0.5 mm, by which dynamic oscillatory excitation was applied to the tested samples that filled the gap between two plates. An electromagnet attached to the rheometer was used to generate magnetic field, perpendicular to the shear flow within the gap. Several different excitation current were applied with the conversion to magnetic flux density being B = 220 I (mT). In order to eliminate the pre-shear history and to distribute the particles evenly, a pre-conditioning shear was conducted prior to each test run. The pre-conditioning run was a constant shear of 10 s^{-1} under zero field condition for 1 minute.

3. Experimental Results

3.1. Steady Shear Test

In order to compare the ability of shear thickening of the original medium (the shear thickening mixture of 25 wt% silica in ethylene glycol base) as well as the effect of the addition of iron particles, the steady shear experiments were conducted on both the base fluid and the fabricated MRSTF in a stress sweep manner. It was clear to see in Fig. 1 that the viscosity of the shear thickening base fluid exhibited an obvious upsurge upon a critical stress value. Besides, as it is also presented in Fig. 1, same experiments

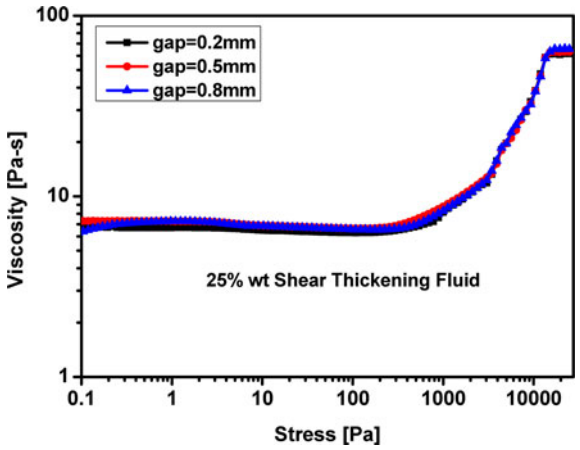

Fig. 1. (Color online) Stress *vs.* viscosity of 25 wt% shear thickening fluid under different plate gaps.

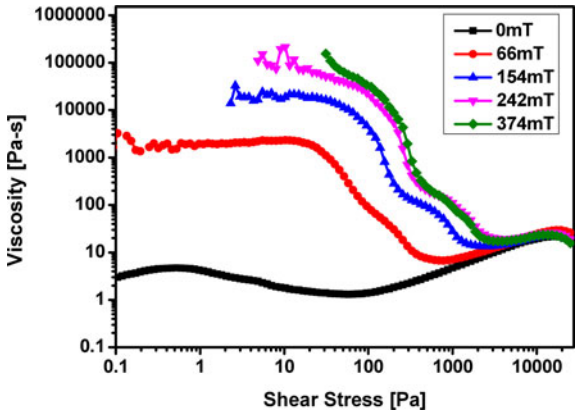

Fig. 2. (Color online) Stress Sweep of 5 wt% MRSTF under varied external field conditions.

over the same original shear thickening fluid medium were carried out with great repeatability, while varied gaps (0.2 mm, 0.5 mm, and 0.8 mm) between the parallel plates of the rheometer were adopted, thus eliminating inertial as possible reason for the increase of the viscosity. This result agrees with a number of publications which have already reported such an experiment outcome.

Now that the steady shear response of the original STF is examined and confirmed, the effect of the iron particle addition should also be scaled. As it is given in Fig. 2, the relationship between shear stress and liquid viscosity under augmented magnetic fields is presented. We can see that when the magnetic field was absent, the curve of the MRSTF could exhibit shear thickening behavior at nearly the same critical shear stress point as the original STF, despite the fact that the addition of iron particles might down-scale the actual values. Then with the increasing external magnetic field, as observable from the chart, the onset of shear thickening points were pushed to higher stress values. Moreover, the curves of different field conditions could always rejoin the zero-field curve after a minimum viscosity was exhibited with a smaller range of overlapping as the magnetic density increased. The experiment's result revealed the fact that the attractive magnetization dipolar force could be applied to mask or control the onset of the shear thickening behavior as additional yield stress was triggered due to magneto-rheology (Brown *et al.,* 2010). This phenomenon was enhanced by our MRSTF, the range of the controllability of shear thickening behavior, as revealed in Fig. 2 was quite extensive and up to magnetic saturation point. With that we could come to the conclusion that the MRSTF being discussed here showed the dual function of magneto-rheology and shear thickening, and the magnetic sensitive iron particles in this system provided us with a pathway to maneuver the scale of shear thickening by applying varied magnetic field densities. In the following subsections that follow, we would unfold the discussion to show dynamic situations and present the viscoelastic property of MRSTF under different variables like strain amplitude, frequency and external field through the LAOS test.

3.2. Strain Amplitude Dependence

The strain amplitude dependence of both storage (G′) and loss moduli (G″) were investigated under varied external magnetic fields with the strain amplitude sweeping from 0.01% to 100% at a constant frequency value of 5 rad/s. The experimental curves of 5 wt% sample are shown in Fig. 3. It is observed that the dynamic parameters for MRSTF without magnetic field was quite different from the occasions when the magnetic fields were applied, an obvious MR effect was displayed with a pronounced increase of several orders of magnitude. Moreover, G′ for the MRSTF sample (Fig. 3a) without external magnetic field was constant for a large range of strain amplitude variation till approximately 10% before a slight decrease was recorded. As for the occasions where magnetic field was applied, G′ of the MRSTF sample displayed relatively shorter periods of plateau and then started to decrease at small deformations with the increase of external magnetic field. A series of critical strains, here defined as γ_c, were thus used to signal the plateau periods of the 5 wt% MRSTF sample at different external field strengths. This is to say the strain dependent viscoelasticity of the MRSTF sample was sensitive to external field condition. This effect is considered to be a consequence of the dismantling of particle chains when strain deformation is beyond a critical strain value of γ_c, which is used to signal the transition point of LVE and NLVE range for viscoelastic materials. When the actual deformation falls in the range from zero to specific critical strain γ_c, the microstructure of viscoelastic material is considered stable and intact,

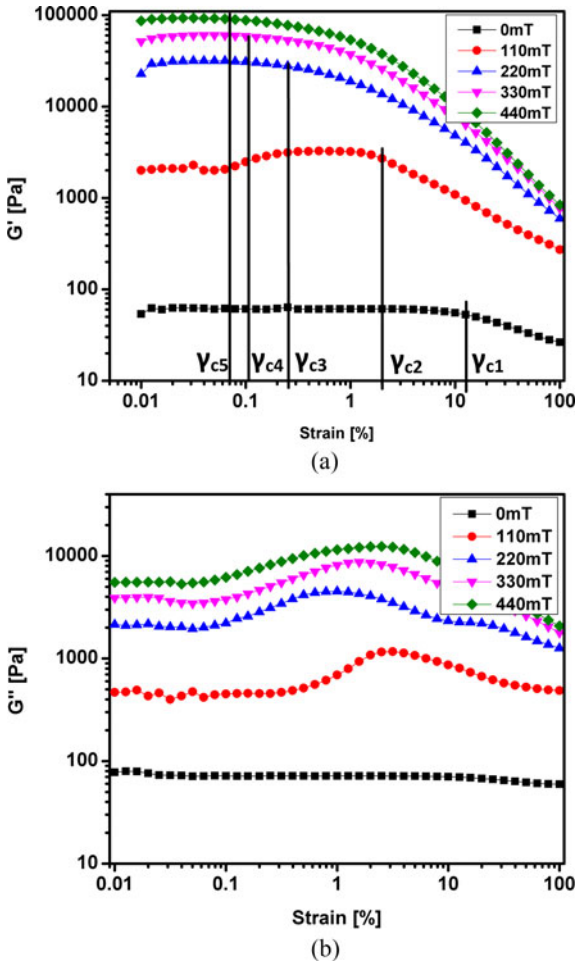

Fig. 3. (Color online) G′ and G″ variation with strain sweep range 0.01-100% at 5 rad/s frequency for 5 wt% sample.

thus exhibits constant G′ value. Conversely, when the strain amplitude is higher than this LVE range, the microstructure is destroyed and the NLVE regime is shown. The loss modulus G″ of the MRSTF sample also exhibited a plateau for small strain amplitudes, and then it increased steadily to a local maximum value before it decreased gradually, as it is shown in Fig. 3b.

Investigating further into the comparison of G′ and G″ of the MRSTF samples, Fig. 4 gives strain sweep results for 5 wt% sample with external magnetic flux density being 220 mT, it is observed that storage modulus decreases from small deformation, and the loss modulus increase to a local maximum before decreasing, a crossover point where loss modulus outweighs storage modulus is displayed at comparatively high strain amplitude. This result is not accidental, as other tests given in Fig. 3 are found to present a conformed trend. This phenomenon is usually referred to as weak strain overshoot (Hyun *et al.,* 2011), and is connected to a typical MRF response in many ways (Li *et al.,* 2004).

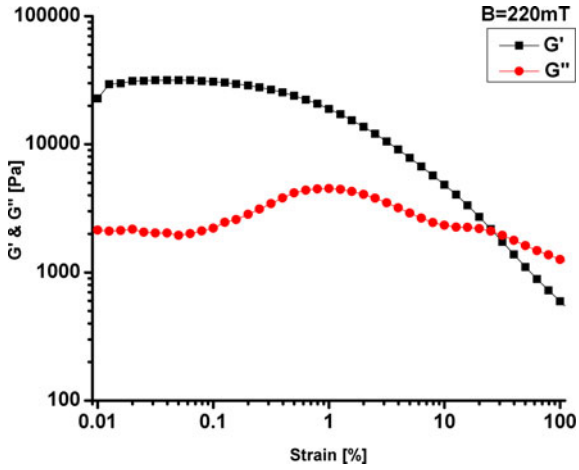

Fig. 4. (Color online) G′ and G″ comparison with strain sweep range 0.01-100% at 5 rad/s frequency for 5 wt% sample when the external magnetic flux density is 220 mT.

The pronounced local maximum in loss modulus signals a remarkably robust feature of soft glassy materials, the MRF is categorized in such domain (Hyun *et al.,* 2011). If we consider modulus increase as a result of network formation and decrease as a consequence of network destruction, then the local maximum loss modulus means the balance between formation and destruction is more dominant in the formation aspect until the structure destruction parameter overtakes it. One plausible explanation given to the G″ overshoot is that the microstructure established at early oscillatory deformation is destroyed and reformed at high strain deformation (Sim *et al.,* 2003). What is also worth noting is that the 5 wt% MRSTF sample shows no thickening behavior, which features in both G′ and G″ increase at high strain amplitude (Hyun *et al.,* 2002). This is on one hand due to the fact that actual shear rate of oscillatory test is not so high to trigger the shear thickening phenomenon, and on the other hand is explained by the fact that the thickening behavior is suppressed in the mixture system (Zhang *et al.,* 2008; Brown *et al.,* 2010).

With what is mentioned above, we can conclude to a certain extent that the fabricated MRSTF samples behaved more like MRF under oscillatory test when the external magnetic field is applied. This could also be proven by experimental result with MRF, which is mixture of same iron particles and simple Newtonian fluid of silicone oil.

Another method that is also used to determine the LVE range is by investigating the shear stress response and strain amplitude level within one oscillatory cycle (Lakes, 2009). It is proposed that the hysteresis loop for strain-stress would be elliptical in case of sinusoidal loading when the strain amplitude is within the LVE range, and gives rise to a non-elliptical shape due to higher

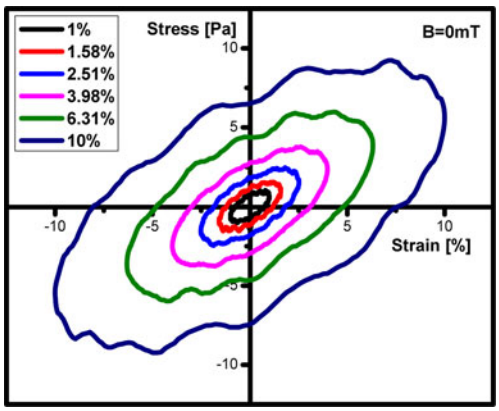

Fig. 5. (Color online) Strain-stress relation of 5 wt% MRSTF under zero field condition.

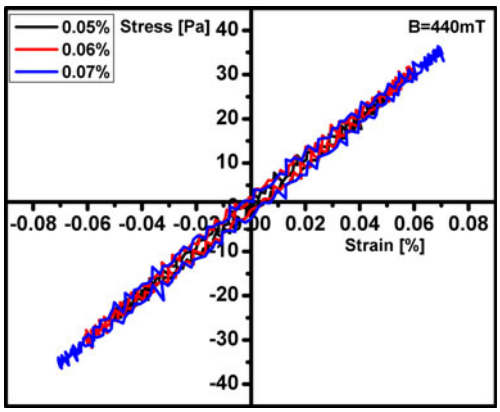

Fig. 6. (Color online) Linear strain-stress relation of 5 wt% MRSTF under field condition.

harmonics distortion when the excitation is beyond linear viscoelastic (LVE) range.

The stress-strain loops of the 5 wt%. MRSTF sample under different strain amplitude in a period when the external magnetic field is not applied are presented in Fig. 5. It is clear to see that the stress-strain loops for MRSTF without a magnetic field were elliptical in shape when the strain amplitude ranged up to 10%. This phenomenon demonstrates that the MRSTF could be referred to as LVE material within the strain range of 0-10%, which was a consistent result as is mentioned previously in a strain sweep test.

As a comparison, the LAOS test result of MRF is often presented in rectangular shape as given in rectangular shape (Deshmukh and McKinley, 2004). It could be concluded that even though the MRSTF sample exhibited a lot in common with typical MRF (mixture of 5 wt% iron particles and silicone oil), there are involved obvious differences. The current MRSTF material showed observable slope with the ellipse loop, which demonstrated sound stiffness, while no such slope could be detected with MRF under zero field condition.

Furthermore, the strain-stress relationship of 5 wt% MRSTF under the condition of external magnetic field was studied. From Fig. 6, we could see that when the strain was within the linear regime, as was found in the strain sweep tests, the strain-stress hysteresis loops exhibited an ellipse in shape, yet the area of the loop as well as the slope between main axis and x-axis maintained approximately the same value. This phenomenon indicated that when the material was deformed under LVE range the damping capacity was not a function of external strain input and the stiffness was also independent of that very variable parameter. Therefore it reflected a conformed result of constant moduli in linear range under the configuration of strain sweep tests. As for the MRF sample, the hysteresis loop was found to be effectively assembled due to the fact

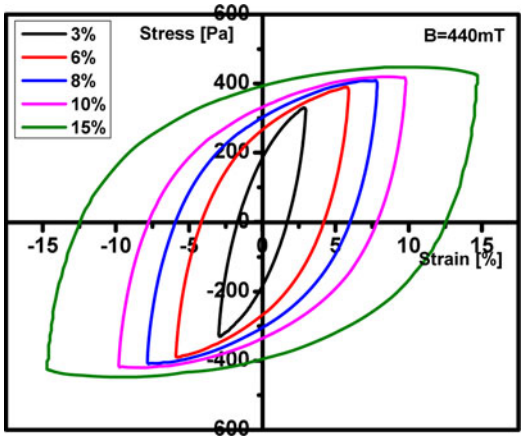

Fig. 7. (Color online) Transition of linearity and non-linearity for 5 wt% MRSTF under external magnetic field.

that the iron particles were forming the same gap-spanning structure and were not ruptured for both kinds of liquid samples within the linear range.

Further comparison of the strain-stress relationship was presented in Fig. 7 where the strain amplitudes were considerably larger and extended to NLVE range. From this figure it was found that the stress response against strain amplitude could still maintain its elliptical shape when the scale was up to 6% before gradually deforming into an irregular shape, for instance, at the strain amplitude of 15%. It is worthwhile pointing out that this set of hysteresis loops exhibited notable difference compared to the result presented in Fig. 6, even though the loops appeared linear. It was observed that the slope between the main axis and x-axis decreased with the increasing strain amplitude and the area of loop increased with the increase of deformation, this phenomenon signals variable damping capacity and stiffness against strain amplitude under certain external magnetic field. The observed phenomenon means that the nonlinear behavior might not be observed

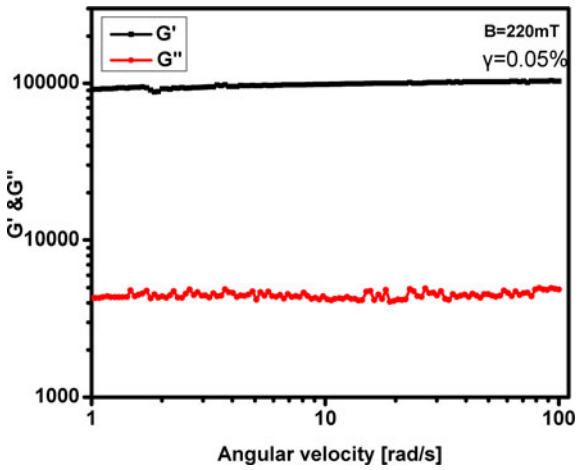

Fig. 8. (Color online) Storage and loss moduli versus angular frequency when strain is 0.05%, B = 220 mT.

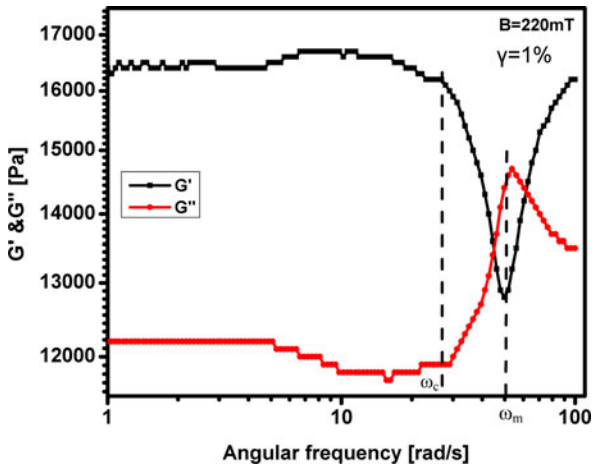

Fig. 9. (Color online) Storage and loss moduli versus angular frequency when strain is 1%, B = 220 mT.

immediately after the microstructure was destroyed. The MRSTF could still maintain linear response when the microstructure was partially destroyed even though the dynamic performance like storage and loss moduli have already shown significant effect upon the destruction of microstructure (Gong *et al.,* 2012). While in the case of the MRF the loops for the MRF were approaching nearly rectangular shape, which meant limited variation on stiffness in non-linear visco-elastic range.

With the description, we can conclude that the MRSTF possesses linear viscoelastic (LVE) range of 0 - 0.1%, even though an elliptical stress response could also be observed at an early stage of non-linear regime, which demonstrated that the very material was prone to maintain the linear response until initial microstructure was completely raptured. And the key criterion in deciding the actual transition point is to examine the strain dependence of damping capacity and stiffness of the material.

3.3. Frequency Dependence

Apart from the strain amplitude examination, frequency is another factor that influences the dynamic rheological performance of viscoelastic materials. Fig. 6 gives the frequency sweep test result for moduli comparison from 1-100 angular frequency at small constant deformation of 0.05%, which is supposed to be within the linear viscoelastic range as shown in Fig. 3. This figure shows that the storage modulus increased slightly with the increase of angular frequency, whereas the loss modulus remained more or less the same in the frequency sweep range. Also the storage modulus was higher than loss modulus in the entire range, which indicated that the MRSTF was of predominantly elastic response in the angular frequency range of 1-100 rad/s.

The effect of angular frequency inputs on MRSTF performance when the strain amplitude is beyond the LVE range is presented in Fig. 9.

In Fig. 9, we can see that at low frequencies the storage modulus G′ exhibited an approximate plateau value until a certain frequency, then G′ decreased gradually with the increasing frequency. The frequency point at which G′ started to decrease is defined as critical frequency ω_c. With the frequency increasing further, G′ displayed a local minimum at a frequency value ω_m, then started to increase again. In contrast the loss modulus G″ increased gradually until the frequency point ω_m then started to decrease. This phenomenon shares much similarity with MRF (Li *et al.,* 2004), and is also a direct evidence of microstructural variation of the MRSTF under different driving frequencies.

The experimental can be explained in this way:

When the frequency is low, the dynamic shear rate, which is defined as $\omega\gamma$, is at very low level, thus the microstructure of the MRSTF did not experience obvious change. In this situation, the hydrodynamic forces could not be compared to chain-chain interactions that constitute the microstructure of MRSTF, thus the storage modulus G′ which represents the elastic component of the viscoelastic material is of near constant value at small frequency ranges. When the frequency value increased to ω_c, the microstructure of MRSTF started to break due to the increasing dynamic shear rate, which caused the decrease of G′. However, when the driving frequency was increasing to higher level, for instance ω_m, the oscillatory deformation was applied to the material at a fairly fast rate and that should leave limited time for the structure to either rearrange or break. Then the magneto-static forces started to take dominant role in the microstructural interactions, and led to the fact that G′ increased gradually after a certain frequency was surpassed. This experimental result once again confirm the conclusion that the MRSTF behaves quite

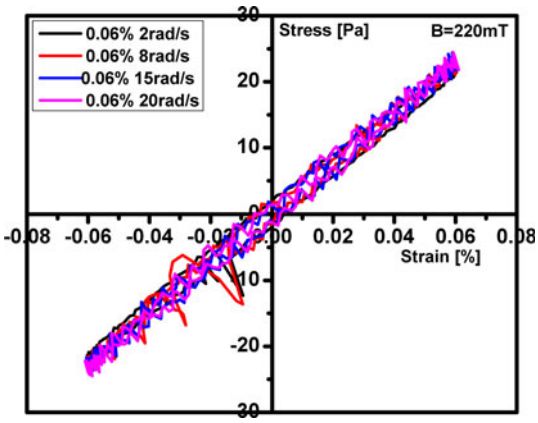

Fig. 10. (Color online) Strain-Stress hysteresis loop under different frequency when strain is 0.06%, B = 220 mT.

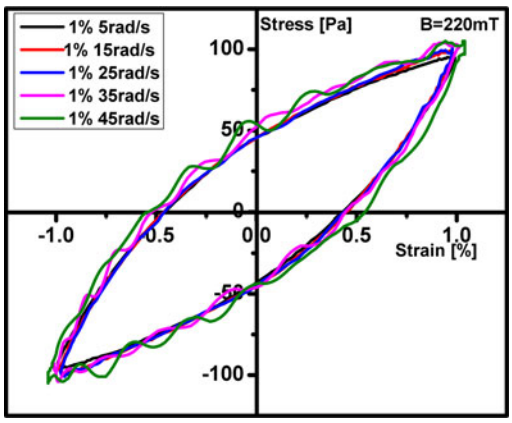

Fig. 11. (Color online) Strain-Stress hysteresis loop under different frequency when strain is 1%, B = 220 mT.

assemble to MRF in the case of dynamic oscillatory shear.

The stress-strain loops for MRSTF sample at different frequency when strain amplitude is 0.06%, which is within the linear range, are represented in Fig. 10. From this figure, we can see that the loops did not show much difference with either damping capacity or stiffness when the strain amplitude was within linear regime. This result provides sound proof with the frequency sweep tests described earlier.

The stress-strain loops for MRSTF sample at different frequency when strain amplitude is 1%, which falls in the non-linear range, are represented in Fig. 11. From this figure, we can see that the loops did not show much difference with either damping capacity or stiffness with the variation of angular frequency. The elliptical shape was maintained until the frequency was at a relatively high level of 35 rad/s, which is a compatible result with ω_c shown in Fig. 9. Comparing the hysteresis loops of varied angular frequency within or beyond the LVE range, we can come to the conclusion that the material's mechanical performance is independent of angular frequency change.

3.4. Field dependence

The magnetic field dependence of MRSTF can be easily analyzed by setting the material at fixed strain amplitude and driving frequency. Fig. 12 gives the strain-stress loops of MRSTF under augmented levels of magnetic fields when the strain amplitude was set as 0.07% at a constant frequency of 5 rad/s. It was seen from this figure that the slope of main axis and x-axis was dependent on the external magnetic field, while the overall shape as well as the area of hysteresis loops did not change significantly over the variation of magnetic fields. The experimental results revealed that the magnetic field was not the factor that introduces non-linearity and changes in overall damping performance, but was able to control the material's stiffness within the LVE range.

The field dependence of MRSTF when the strain

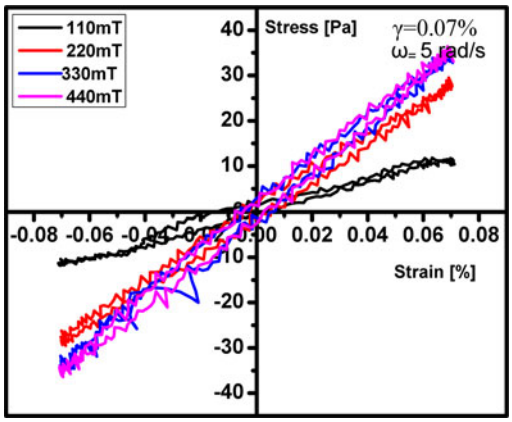

Fig. 12. (Color online) Field dependence of MRSTF under fixed strain of 0.07% and frequency of 5 rad/s.

amplitude is in the NLVE range of 1% under the oscillation of 5 rad/s is given in Fig. 13. From this figure, the loop shapes are all perfect ellipses, which is a consistent result that the MRSTF is able to maintain linear stress response before the microstructure is fully destroyed, when the external excitations either physical or magnetic are of intermediate level. Likewise, the experiment also indicated the result that the magnetic field could not introduce non-linearity, but was able to control the material's stiffness and overall damping performance, which is comparable with the facts in the tests within the LVE range (Fig. 12).

3.5. MRSTF modeling

3.5.1. Four-parameter viscoelastic model

The experimental results, shown in previous sections, indicate the relation between stress response and input strain amplitude as well as their strain, frequency and magnetic dependence. These descriptions reveal the viscoelastic properties of MRSTF. Previously, the viscoelastic properties of MR and ER fluids were studied intensively through

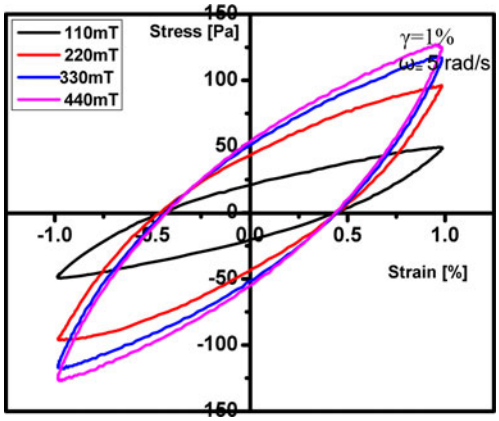

Fig. 13. (Color online) Field dependence of MRSTF under fixed strain of 1% and frequency of 5 rad/s.

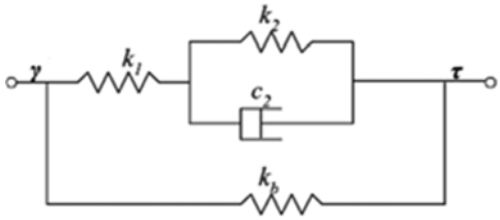

Fig. 14. Four parameter viscoelastic model.

Table 1. Identified parameters (strain: 1%).

Flux density	k_b (kPa)	k_1 (kPa)	k_2 (kPa)	c_2 (kPa-*s*)
110 mT	2.0837	57.7647	9.4899	19.8832
220 mT	3.7503	113.5787	11.0573	38.2406
330 mT	4.8035	133.3120	18.3388	48.7305
440 mT	5.2437	146.32	29.6564	55.3819

experimental and modeling approaches (Li *et al.,* 2002; Li *et al.,* 2003). Compared with ER and MR fluid, the MRSTF material exhibits field dependent modulus and damping capability, thus a four parameter viscoelastic model developed in (Li *et al.,* 2010) as shown in Fig. 14, which extended the classical three-parameter standard solid model, is applied to model the rheological behavior of MRSTF.

In this model, k_1, k_2 and c_2 constitute standard viscoelastic solid model, which describes damping capacity of the model, while the field dependence of modulus is expressed in the parameter k_b. The strain amplitude is γ, and the response stress is presented by τ, the strain-stress relationship is given in Eq. (1).

$$\tau = (G' + iG'')\gamma, \tag{1}$$

where G' and G'' are respectively real and imaginary parts of complex modulus and can be derived in following method (Zhu and Liu 1996)

$$G' = \frac{(k_1k_2 + k_1k_b + k_2k_b)[(k_1+k_2)^2 + c_2^2\omega^2] + c_2^2\omega^2k_1^2}{(k_1+k_2)[(k_1+k_2)^2 + c_2^2\omega^2]} \tag{2}$$

$$G'' = \frac{c_2\omega k_1^2}{[(k_1+k_2)^2 + c_2^2\omega^2]}. \tag{3}$$

In this set of equations ω is the driving frequency of the oscillatory shear test, in which the input strain is in a harmonic form. For a harmonic strain input with an amplitude of g_0, the stress response is obtained as

$$\tau(t) = \gamma_0\sqrt{G'^2 + G''^2}\sin(\omega t + \varphi), \tag{4}$$

where φ is the phase lag between the input and output, which is calculated by $\varphi = \tan^{-1}(G''/G')$.

3.5.2. Parameter identification

Based on Eq. (5), the relationship between strain input and stress output is established, and the moduli G' and G'', which are involved in the calculation, could be determined by fitting the four unknown parameters based on the method of least squares minimization on the platform of Matlab. In this optimization process, the model-predicted stress is given by Sm and the actual experimental data is Se, and the objective function is thus proposed as

$$J = \sum_{i=1}^{N}(Sm(i)^2 - Se(i)^2)^2, \tag{5}$$

where N is the number of experimental data in one loop. In the optimization process, the smaller the value for objective function, the more accurate the estimation for the parameters is.

Different sets of the four parameters were estimated for different experimental conditions. The parameter values for four different current inputs and constant strain amplitude of 1% are presented in Table 1. From the result of the identified results, all four parameters increase steadily with the increase of external magnetic field, which demonstrated field dependence same as shown in experimental results. Especially, the parameter k_b, which is related to the field dependence of modulus, increase from around 2 kPa at 110 mT to 5 kPa at 440 mT, the parameters evolution with respect to external magnetic fields are presented in Fig. 13. From the curves given in these figures, the field dependence is clearly defined. This phenomenon demonstrated that the external field could alter stiffness of MRSTF material, and this is a conformed result to Fig. 13.

With the resultant estimated parameters from the optimization process, we could also virtually reconstruct the strain-stress relationship and have it compared with the experimental data. The comparisons are presented in Fig. 16. It is seen that the plots from the four parameter model can reflect the experimental results at different magnetic fields with acceptable accuracy.

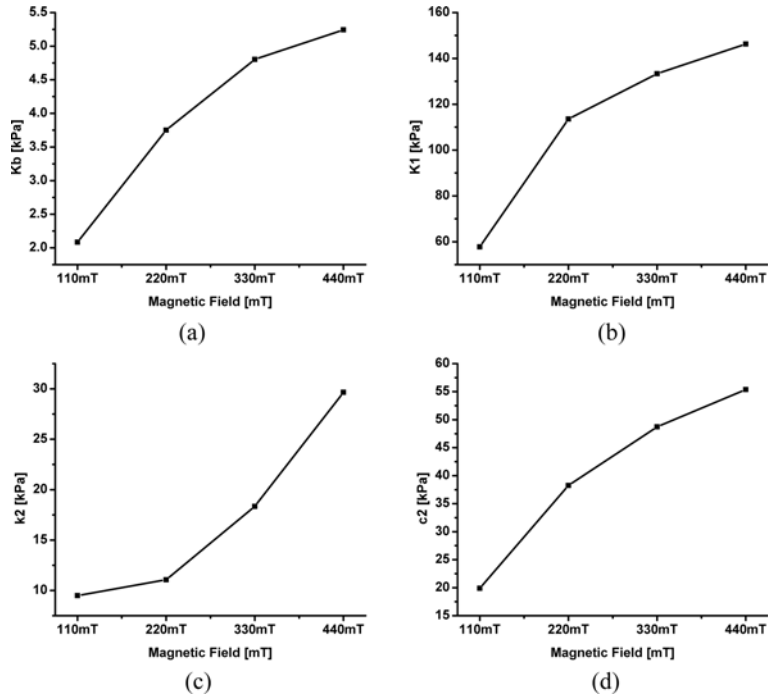

Fig. 15. Parameters variation with respect to external magnetic field.

4. Conclusions

In this research, oscillatory tests featuring strain amplitude variation and frequency changes are applied to the MRSTF sample under different levels of external magnetic fields. The LVE and NLVE response for system are defined and analyzed.

It is found that in this dynamic experimental setting, the strain amplitude should be considered as the factors that bring about non-linearity to the target viscoelastic material as well as the mechanical behavior. The external magnetic field is the factor changing the system stiffness rather than non-linearity.

From the oscillatory experimental setting applied in this work, the fabricated mixture system of MRSTF exhibited strain and frequency dependence that is quite assemble to MRF, which indicates that the MR effect has a dominant role when iron particles are introduced to STFs under dynamic excitation where actual shear rate might not be sufficient to trigger shear thickening effect.

A four-parameter viscoelastic model was used to describe the performance of MRSTF. It is clearly demonstrated that the parameters of the four-parameter viscoelastic model that were identified possessed a tendency to increase with the magnetic field. The comparison between the experimental results and the model-predicting values demonstrates that the model could represent the MRSTF performance effectively.

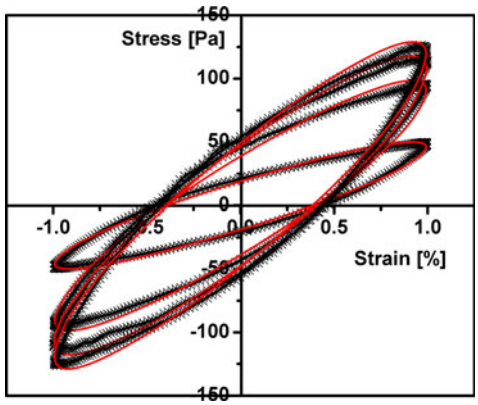

Fig. 16. (Color online) A comparison between experimental data and model-predicted results with the input strain amplitude being 1%.

Acknowledgements

This work is partially supported by DSTO Fellowship program from the Defense Science and Technology Organisation, Australia, and the “General Collaborative Research Project 2013” scheme, IFS, Tohoku University.

References

Ahn, K.H., K.S. Cho, K. Hyun, and S.J. Lee, 2005, A geometrical interpretation of large amplitude oscillatory shear response, *J. Rheol.* **49**, 747-758.

Bender, J.W. and N.J. Wagner, 1995, Optical Measurement of the

Contributions of Colloidal Forces to the Rheology of Concentrated Suspensions, *J. Colloid Interf. Sci.* **172**, 171-184.

Brown, E., N.A. Forman, C.S. Orellana, H. Zhang, B.W. Maynor, D.E. Betts, J.M. de Simone, and H.M. Jaeger, 2010, Generality of shear thickening in dense suspensions, *Nat. Mater.* **9**, 220-224.

Carlson, J.D., D.M. Catanzarite, K.A. St. Clair, 1995, *Fifth International Conference on ER Fluids, MR Suspensions and Associate Technology*, University of Sheffield.

De Vicente, J., D.J. Klingenberg, and R. Hidalgo-Alvarez, 2011, Magnetorheological Fluids: a Review, *Soft Matter* **7**, 3701-3710.

Deshmukh, S.S. and G.H. McKinley, 2004, Rheological Behavior of Magnetorheological Suspensions under Shear, Creep and Large Amplitude Oscillatory Shear (LAOS) flow, *Proc. XIVth International Congress on Rheology,* The Korean Society of Rheology, Seoul.

Dong, S.F., K.Q. Lu, J.Q. Sun, and K. Rudolph, 2006, Adaptive force regulation of muscle strengthening rehabilitation device with magnetorheological fluids, *IEEE T. Neur. Sys. Reh.* **14**, 55-63.

Egres, R.G., F. Nettesheim, and N.J. Wagner, 2006, Rheo-SANS investigation of acicularprecipitated calcium carbonate colloidal suspensions through the shear thickening transition. *J. Rheol.* **50**, 685-709.

Fischer, C., S.A. Braun, P.E. Bourban, V. Michaud, C.J.G. Plummer, and J.A.E. Manson, 2006, Dynamic properties of sandwich structures with integrated shear-thickening uids, *Smart Mater. Struct.* **15**, 1467-1475.

Gong, X.L., Y.G. Xu, S.H. Xuan, C.Y. Guo, and L.Z. Zong, 2012, The investigation on the nonlinearity of plasticine-like magnetorheological material under oscillatory shear rheometry, *J. Rheol.* **56**, 1375-1391.

Hyun, K., S.H. Kim, K.H. Ahn, and S.J. Lee, 2002, Large amplitude oscillatory shear as a way to classify the complex fluids, *J. Non-Newt. Fluid* **107**, 51-65.

Hyun, K., M. Wilhelm, C.O. Klein, K.S. Cho, and J.G. Nam, 2011, A review of nonlinear oscillatory shear tests: Analysis and application of large amplitude oscillatory shear (LAOS), *Prog. Polym. Sci.* **36**, 1697-1753.

Jolly, M.R. and J.W. Bender, 2006, Field responsive shear thickening uid US Patent Application Publication 2006/ 0231357 A1.

Kalman, D.P., 2010, *Microstructure and rheology of concentrated suspensions of near hard-sphere colloids*, Ph.D. thesis, University of Delaware.

Kikuchi, T., K. Otsuki, J. Furusho, H. Abe, J. Noma, and M. Naito, 2011, Development of a compact Magnetorheological Fluid Clutch for Human-Friendly Actuator, *Advanced Robotics* **25**, 1362.

Kim, S.H., H.G. Sim, K.H. Ahn, and S.J. Lee, 2002, Large Amplitude Oscillatory Shear Behavior of Network Model for Associating Polymeric Systems, *Korea-Aust. Rheol. J.* **14**, 49-55.

Lakes, R., 2009, *Viscoelastic Materials*, Cambridge University Press, New York.

Li, W.H., H. Du, and N.Q. Guo, 2004, Dynamic behavior of MR suspensions at moderate flux densities, *Mater. Sci. Eng. A* **371**, 9-15.

Li, W.H., Du, H., Chen, G., S.H. Yeo, and N.Q. Guo, 2002, Nonlinear rheological behavior of MR fluids: step strain experiments, *Smart Mater. Struct.* **11**, 209-217.

Li, W.H., Du, H., Chen, G., S.H. Yeo, and N.Q. Guo, 2003, Nonlinear viscoelastic properties of MR fluids under large-amplitude oscillatory shear. *Rheol. Acta* **42**, 280-286.

Li, W.H., Y. Zhou, and T.F. Tian, 2010, Viscoelastic properties of MR elastomers under harmonic loading, *Rheol. Acta* **49**, 733-740.

Liu, Y.D., J. Lee, S.B. Choi, and H.J. Choi, 2013, Silica-coated carbonyl iron microsphere based magnetorheological fluid and its damping force characteristics, *Smart Mater Struct.* **22**, 065022

McKinley, G.H., R.H. Ewoldt, and A.E. Hosoi, 2008, New measures for characterizing nonlinear viscoelasticity in large amplitude oscillatory shear, *J. Rheol.* **52**, 1427-1458.

Milecki, A. and M. Hauke, 2012, Application of magnetorheological fluid in industrial shock absorbers, *Mech. Syst. Sig. Pr.* **28**, 528-541.

Neagu, R.C., P.E. Bourban, and J.A.E. Manson, 2009, Micromechanics and Damping Properties of Composites Integrating Shear Thickening Fluids, *Compos. Sci. Technol.* **69**, 515-522.

Ng, T.S.K., G.H. McKinley, and R.H. Ewoldt, 2011, Large amplitude oscillatory shear flow of gluten dough: A model power-law gel, *J. Rheol.* **55**, 627-654.

Park, B.J., F.F. Fang, H.J. Choi, 2010, Magnetorheology: materials and applications, *Soft Matter* **6**, 5246-5253.

Petekidis, G., F. Renou, and J. Stellbrink, 2010, Yielding processes in a colloidal glass of soft star-like micelles under large amplitude oscillatory shear (LAOS), *J. Rheol.* **54**, 1219-1242.

Rankin, P.J., A.T. Horvath, and D.J. Klingenberg, 1999, Magnetorheology in viscoplastic media, *Rheolo. Acta* **38**, 471-477.

Russo, R. and M. Terzo, 2011, Design of an adaptive control for a magnetorheological fluid brake with model parameters depending on temperature and speed, *Smart Mater. Struct.* **20**, 115003.

Sim, H.G., K.H. Ahn, and S.J. Lee, 2003, Three-dimensional dynamics simulation of electrorheological fluids under large amplitudes oscillatory shear flow, *J. Rheol.* **47**, 879-95.

Sun, W.X., Y.R. Yang, T. Wang, C.Y. Wang, X.X. Liu, and Z. Tong, 2011, Large amplitude oscillatory shear rheology for nonlinear viscoelasticity in hectorite suspensions containing poly(ethylene glycol), *Polymer* **52**(6), 1402-1409.

Wang, S.Q., X. Li, and X.R. Wang, 2009, Nonlinearity in large amplitude oscillatory shear (LAOS) of different viscoelastic materials, *J. Rheol.* **53**, 1255-1274.

Yu,T., J.L. Jiang, Y.G. Meng, and S.Z. Wen, 2010, A shear thickening phenomenon in magnetic field controlled-dipolar suspensions, *Appl. Phys. Let.* **97**, 151904

Zhang, X., W. Li, and X.L. Gong, 2008, Study on magnetorheological shear thickening fluid, *Smart Mater. Struct.* **17**, 015051.

Zhu, G. and X. Liu, 1996, *Theory of viscoelasticity*, The Press of the University of Science & Technology of China, Hefei.

Zhu, X.C., X.J. Jing, and C. Li, 2012, Magnetorheological Fluid Dampers: A Review on Structure Design and Analysis, *J. Intel. Mat. Syst. Str.* **23**, 839-873.